Research Article

Qing Zhang, Zongfeng Sha, Xun Cui, Shengqiang Qiu*, Chengen He, Jinlong Zhang, Xianggang Wang, and Yingkui Yang*

Incorporation of redox-active polyimide binder into $LiFePO_4$ cathode for high-rate electrochemical energy storage

https://doi.org/10.1515/ntrev-2020-0092
received November 4, 2020; accepted November 17, 2020

Abstract: Commercial $LiFePO_4$ (LFP) electrode still cannot meet the demand of high energy density lithium-ion batteries as a result of its low theoretical specific capacity (170 mA h g^{-1}). Instead of traditional electrochemical inert polyvinylidene fluoride (PVDF), the incorporation of multifunctional polymeric binder becomes a possible strategy to overcome the bottleneck of LFP cathode. Herein, a novel polyimide (PI) binder was synthesized through a facile hydrothermal polymerization route. The PI binder exhibits better connection between active particles with uniform dispersion than that of PVDF. The multifunctional PI binder not only shows well dispersion stability in the organic electrolyte, but also contributes to extra capacity because of the existence of electrochemical active carbonyl groups in the polymer chain. Besides, the high intrinsic ion conductivity of PI also results in promoted ion transfer kinetic. Consequently, the LFP cathode using PI binder (LFP–PI) shows larger capacity and better rate capability than LFP cathode with PVDF binder (LFP–PVDF). Meanwhile, the superior binding ability also endows LFP–PI with great cycling stability compared to the LFP–PVDF electrode.

Keywords: lithium-ion batteries, $LiFePO_4$, rate capability, binder, polyimide

* **Corresponding author: Shengqiang Qiu,** School of Chemistry and Materials Engineering, Hunan University of Arts and Science, Changde 41500, China; Graphene R&D Center, Guangdong Xigu Tanyuan New Materials Corporation Limited & South-Central University for Nationalities, Foshan 528000, China, e-mail: qshq2021@huas.edu.cn
* **Corresponding author: Yingkui Yang,** Key Laboratory of Catalysis and Energy Materials Chemistry of Ministry of Education & Hubei Key Laboratory of Catalysis and Materials Science, South-Central University for Nationalities, Wuhan 430074, China; Graphene R&D Center, Guangdong Xigu Tanyuan New Materials Corporation Limited & South-Central University for Nationalities, Foshan 528000, China, e-mail: ykyang@mail.scuec.edu.cn
Qing Zhang, Zongfeng Sha, Xun Cui: Key Laboratory of Catalysis and Energy Materials Chemistry of Ministry of Education & Hubei Key Laboratory of Catalysis and Materials Science, South-Central University for Nationalities, Wuhan 430074, China
Chengen He, Jinlong Zhang, Xianggang Wang: Graphene R&D Center, Guangdong Xigu Tanyuan New Materials Corporation Limited & South-Central University for Nationalities, Foshan 528000, China

1 Introduction

Lithium-ion batteries (LIBs) have covered most of the aspects of human civilization such as various mobile electronic devices, electric vehicles, and large-scale energy storage [1–8]. Compared with $LiCoO_2$, $LiMn_2O_4$, and Li-rich layered cathode, $LiFePO_4$ (LFP) has already dominated the most commercial applications for its excellent cycle stability, high safety, environmental friendliness, and low cost [9,10]. However, the poor electronic conductivity and low ion mobility result in inferior rate capability for the LFP cathode [11,12]. These shortcomings can be improved by the size reduction to the nanoscale, carbon/conductive polymer coating, and element-doping strategies [13–17]. The incorporation of carbon additives during the electrode fabrication process also can effectively promote the electronic conductivity. In addition, the high reversibility and moderate operating potential also make LFP more competitive compared to other cathodes. Therefore, there are still no alternatives available to completely replace the LFP cathode in terms of operational safety, stability, and manufacturing cost. Despite the significant progresses in the past few decades, the energy density of LFP-based batteries has almost reached its limit value because of its low theoretical specific capacity (170 mA h g^{-1}), which seriously impeded the development of high-density LIBs. Therefore, the poor energy density has become a bottleneck restricting further development of LFP.

Generally, it is almost impossible to improve the specific capacity of LFP cathode through the material

modification. Instead, reducing inactive components, increasing active mass loading, and using lightweight package during the electrode fabrication process seem to be the feasible strategies [18,19]. Among the critical electrode components, the current collector and conductive additive that supply continuous and uninterrupted electron transfer channel are almost certainly impossible to be replaced [20–22]. Therefore, optimizing the content and properties of polymeric binder functioning as the bridge between active particles becomes a feasible solution to enhance the energy density [23]. Currently, the commercial binders used in both cathode and graphite anode are dominated by polyvinylidene fluoride (PVDF) as a result of its superior electrochemical stability, mechanical properties, processing properties, oxidation, and corrosion resistance for the high energy C–F bond [24–26]. Nevertheless, the swelling in the electrolyte during long-time operation would result in the failure of binding property, which further causes the isolation and crack of active particles. The binding mechanism of PVDF relies on weak van der Waals force, which cannot withstand the large volume change of electrodes especially for silicon anode [27]. Notably, the poor ion conductivity of PVDF also leads to sluggish ion diffusion and large polarization, further limiting the rate capability. In addition, some other binders such as polytetrafluoroethylene, carboxyl methyl cellulose, polyacrylic acid, and styrene butadiene rubber have also been used in various energy storage systems [23,28]. However, their differences in solubility, dispersion, adhesion strength, conductivity, and electrochemical stability make them only suitable for specific solvent, electrolyte, or voltage window [29–31].

Recently, polyimide (PI) binder has become a promising candidate for LIBs because of its superior thermal/mechanical properties, strong adhesion strength, excellent film-forming ability, and high intrinsic ion conductivity [32]. Kim et al. reported that Si anode prepared with PI binder exhibited twice the capacity retention than that of Si anode with PVDF [27]. The outstanding mechanical stability of PI can effectively buffer the huge volume change of Si anode during repeated discharge/charge process [33,34]. Inspired by the excellent thermal and chemical stability of PI, Song et al. used a fluorinated PI as the binder of high-voltage Li-rich layered oxide cathode (FPI–LMNC) [35]. Because of the strong interaction between $-CF_3$ groups and surface of LMNC, the formed protective layer effectively suppressed the decomposition of active materials at high voltage (up to 4.7 V). Thus FPI–LMNC showed a significantly enhanced cycling stability than that of LMNC electrode prepared with PVDF. Moreover, PI as a widely used engineering plastic with abundant resources and structural diversity also possesses the potential of large-scale application in energy storage [36,37]. Therefore, the exploration of PI binders holds enormous promise for the enhancement of energy density for high-safety LFP cathode. Besides, PI has been mainly synthesized by thermal amination process involving toxic organic solvents and high-temperature procedures [38]. By comparison, the hydrothermal polymerization is an environment-friendly synthetic route with cost-effectiveness as described in our previous work [37,39,40], avoiding the adoption of toxic solvents and harsh conditions.

Herein, a multifunctional PI binder was synthesized through a facile hydrothermal polymerization route and subsequently used in the fabrication process of LFP electrode. The morphology, dispersion, chemical stability in organic electrolyte, and structural stability during long cycles of LFP electrodes fabricated with PVDF (LFP–PVDF) and PI (LFP–PI) binders were investigated and compared in detail. The PI binder not only serves as the effective bridges between active LFP particles but also boosts the uniform distribution of particles. Besides, the high intrinsic ion conductivity of PI can accelerate ion transfer between active LFP particles. More importantly, the active carbonyl groups existing in the PI chain can contribute to the extra capacity based on the reversible enolization reaction. Therefore, LFP–PI exhibits larger capacity and better rate capability compared with LFP–PVDF. Besides, the superior chemical stability of PI binder in organic electrolyte also endows LFP–PI electrode with great cycling stability. This work confirms that the design of multifunctional polymeric binder can break the performance bottleneck of LFP electrode and offers a new view for the development of high energy density LIBs.

2 Experimental

2.1 Materials

LFP powder was purchased from Guangdong Canrd New Energy Technology Co., Ltd. PVDF was purchased from Solvay Co., Ltd. PI was synthesized through a hydrothermal polymerization method using 3,3′,4,4′-benzophenonetetracarboxylic dianhydride (BTDA) and 1-(4-aminophenyl)-2,3-dihydro-1,3,3-trimethyl-1H-inden-5-amine (DAPI) as monomers. In a typical synthesis, equimolar BTDA (1 g) and DAPI were firstly dispersed in 60 mL deionized water under vigorous stirring at 80°C for 2 h. Then the obtained monomer salt was washed by deionized water to remove the unreacted monomer followed by drying process at 60°C. The

as-prepared monomer salt powder was transferred to a Teflon-lined autoclave and kept at 200°C for 12 h. After being cooled to room temperature, the precipitate was collected by vacuum filtration and washed with deionized water. Finally, the PI was obtained after drying at 80°C overnight under vacuum condition.

2.2 Characterization

The morphology was characterized by SU 8010 field emission scanning electron microscope. Powder X-ray diffraction patterns were recorded at room temperature with a D8 Advance diffractometer. Fourier transform infrared spectra (FT-IR) were conducted on a Nexus 470 spectrometer. Thermogravimetric analysis (TGA) was performed on a Mettler Toledo (Switzerland) at a heating rate of 20°C/min in a nitrogen atmosphere.

2.3 Electrochemical measurements

The working electrodes consisted of LFP (80 wt%), conductive carbon SP (10 wt%), and binders (10 wt%) in *N*-methyl pyrrolidone (NMP). The LFP cathodes were prepared with two different binders of PVDF (LFP–PVDF) and PI (LFP–PI), respectively. Meanwhile, the LFP cathodes were also fabricated using the mixture of PVDF and PI as binders with different PI contents of 30, 50, and 70 wt%, namely LFP–PI-0.3, LFP–PI-0.5, and LFP–PI-0.7. The electrolyte was 1 mol/L $LiPF_6$ in 1:1:1 (v/v/v) mixture of ethylene carbonate (EC)/dimethyl carbonate (DMC)/ethyl methyl carbonate (EMC). Coin type half-cells (CR-2032) were assembled under an argon-filled glovebox with lithium foil as the counter electrode and Celgard 2400 porous membrane as the separator. Cyclic voltammetry (CV) was performed on CHI 760 electrochemical workstation within the potential window of 2.5–4.2 V (vs Li/Li^{+}). Charge–discharge tests were performed on a CT2001A battery testing system between 2.5 and 3.7 V (vs Li/Li^{+}). Electrochemical impedance spectroscopy (EIS) tests were conducted in a frequency range from 0.1 Hz to 100 kHz with AC amplitude of 5 mV by CHI 760 electrochemical workstation.

3 Results and discussion

Figure 1a and b shows the molecular structures and FT-IR spectra of commercial PVDF and the as-prepared PI. PVDF exhibits the typical characteristic peaks at 1,400 and 1,180 cm^{-1}, representing the presence of C–F bonds. As for PI binder, the peaks located at 1,780 and 1,720 cm^{-1} are assigned to the asymmetric and symmetric stretching vibration peaks of C–O moieties, respectively. Another strong peak at around 1,373 cm^{-1} corresponds to the absorption peak of C–N. The FT-IR results confirm the

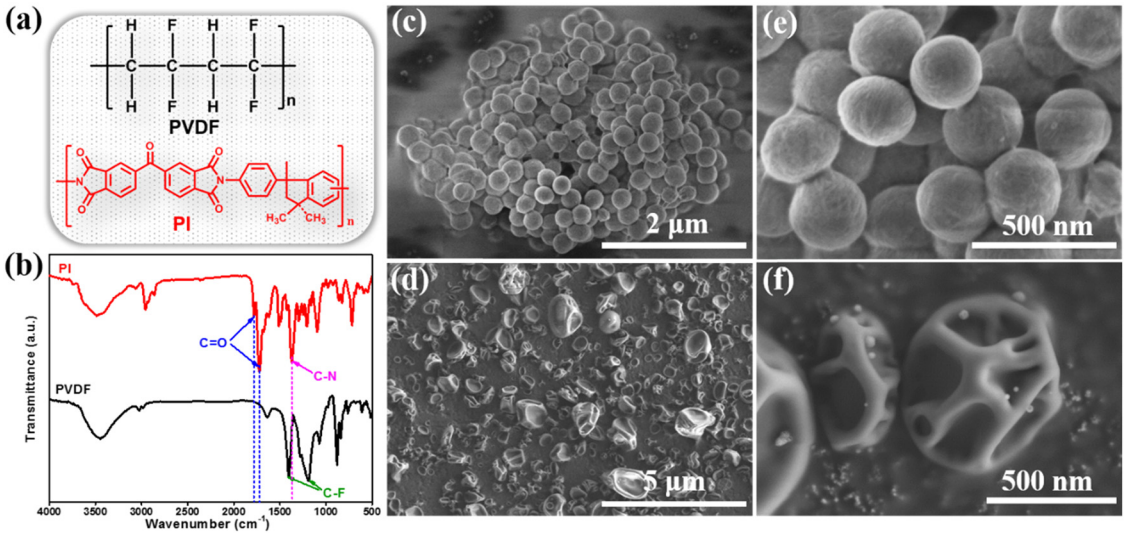

Figure 1: (a) Chain structures and (b) FT-IR spectra of PVDF and PI binders; SEM images of (c and e) PVDF and (d and f) PI binders.

successful synthesis of the targeted PI [41]. The morphologies of PVDF and PI were investigated as shown in Figure 1c–f. The PVDF presents uniform spherical morphology with the average particle size of 200–300 nm (Figure 1c and e). In contrast, the PI appears irregular particles with distinct ridges on the surface, which may be ascribed to the poor symmetry of its molecular structure (Figure 1d and f). The higher degree of disorder with a rougher surface for PI can provide a larger specific surface, thus leading to better binding ability for active materials compared to the regular spherical particles of PVDF.

Figure 2a shows the XRD patterns of PVDF and PI binders. The PVDF shows sharp diffraction peaks because of the regular arrangement of polymer chains because of its symmetrical molecular structure. In contrast, only a bulging peak at about 17° can be observed for PI, which could be explained by the random arrangement of polymer chains with poor crystallinity because of its branch chain existed in the diamine units. TGA curves were also performed to investigate the thermal stability of two binders (Figure 2b). The PI shows high decomposition temperature above 500°C, with a weight loss of only 50 wt% even if the temperature reaches up to 800°C. However, PVDF starts to decompose at about 420°C and quickly degrades to the residual weight of only 30 wt% at 500°C. When the temperature rises to 800°C, complete decomposition almost occurred. The TGA results indicate that PI has a better thermal stability than PVDF, which is mainly because of the enhanced structural stability supported by the strong p–π conjugation resulted from the large amounts of rigid aromatic rings [34,41]. The higher thermal stability of PI binder ensures a wide temperature range, thereby promoting the safety and electrochemical performance of LIBs when used in extremely high temperature environment [42].

The morphology and binding stability of fresh LFP–PVDF and LFP–PI electrode films were further analyzed as shown in Figure 3. Active LFP particles in the LFP–PVDF electrode appear obvious agglomeration and local LFP particles aggregated into micron-sized bulk (Figure 3a and b). Especially, partial LFP particles and conductive carbon are disconnected without PVDF binding (Figure 3c), which may be ascribed to the uneven dispersion during the fabrication process of electrode slurry. LFP–PI electrodes exhibit even distribution of active particles without partial aggregation (Figure 3d and e). In addition, obvious PI binders can be observed between active particles and conductive carbon (Figure 3f). The uniform distribution and better connection of active materials can promote the full infiltration of electrolyte and provide continuous Li-ions diffusion path. Besides, the better binding stability of PI also can effectively avoid re-aggregation of particles during charge–discharge process. The above results reveal that the as-prepared PI can also serve as an effective binder for LFP electrode.

To systematically investigate the influence of different binders on the electrochemical performance of LFP electrode, the coin-type cells with LFP–PVDF and LFP–PI as working electrodes were assembled. Figure 4a shows the typical CV curves of LFP–PVDF and LFP–PI within the same voltage range of 2.5–4.2 V (vs Li/Li^+) at 1.0 mV S^{-1}. LFP–PI and LFP–PVDF show sharp redox peaks at 3.24/3.78 and 3.26/3.66 V, respectively, which are assigned to the typical Li-ions insertion/extraction behavior in LFP electrode [43]. It is worth mentioning that LFP–PI shows significantly larger peak current than that of LFP–PVDF, which can be explained by the higher electrochemical activity of LFP–PI electrode because of the highly intrinsic ion conductivity of PI binder and the uniform distribution of active materials [44]. However, LFP–PI exhibits larger peak potential difference

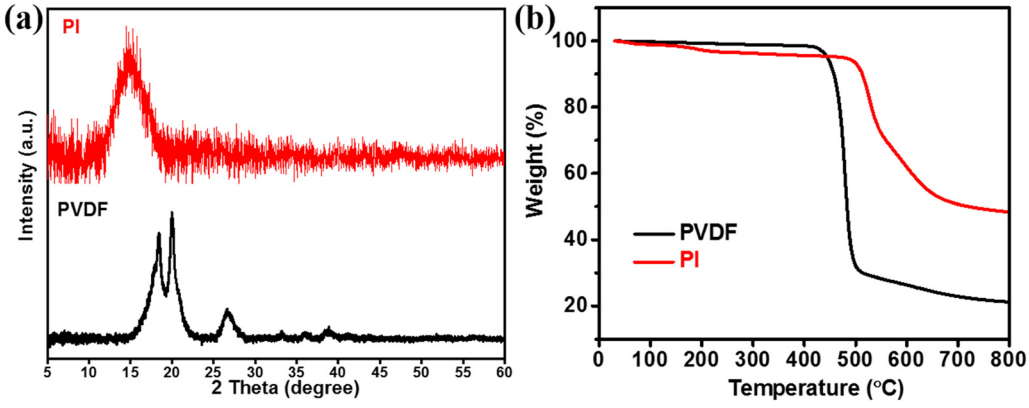

Figure 2: (a) XRD patterns and (b) TGA curves of PVDF and PI binders.

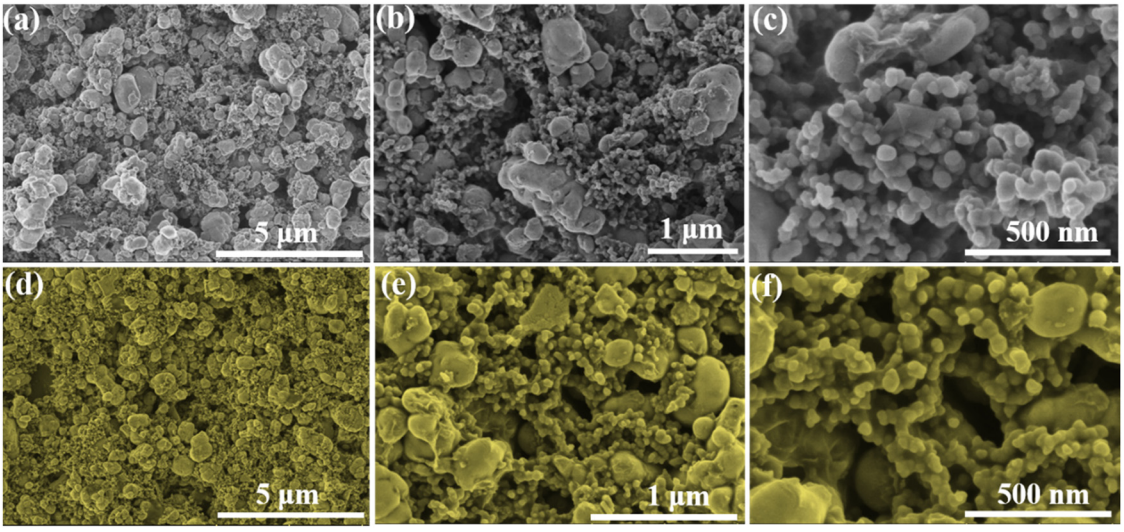

Figure 3: SEM images of fresh (a–c) LFP–PVDF and (d–f) LFP–PI electrode films.

(0.54 V) than that of LFP–PVDF (0.40 V), which may be because of the necessary activation process of PI binder during the initial cycles. Figure 4b shows the rate capabilities of LFP–PVDF and LFP-P. Although they deliver similar reversible capacity at a small rate of 0.2C (1C = 170 mA g^{-1}), LFP–PI shows significantly larger

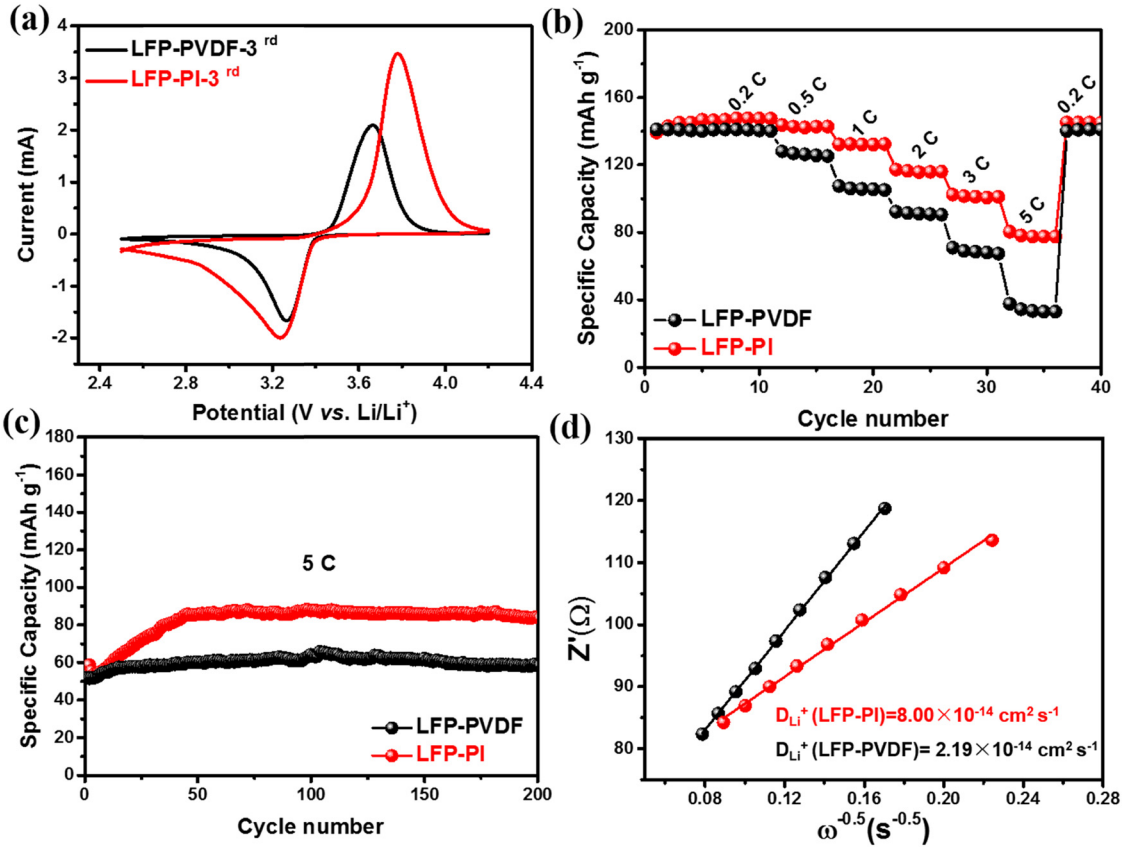

Figure 4: (a) CV curves at 1.0 mV S^{-1}, (b) rate capabilities, (c) cycle performances at 5C, and (d) Li-ion diffusion coefficients (D_{Li}^{+}) of LFP–PVDF and LFP–PI electrodes.

capacity retention of 52.6% than that of LFP–PVDF (23.8%) when the rate increases from 0.2C to 5C, suggesting a much better rate capability. On one hand, the high ion conductivity of PI binder can accelerate the ion transfer between adjacent LFP grains. Besides, the electrochemical activity of PI binder also contributes to extra capacity based on the reversible enolization reaction of carbonyl groups existing in the polymer skeleton [45]. On the other hand, the PVDF binder with electrochemically inert chain structure and poor ion conductivity is unfavorable for the electrochemical performance. Although the LFP–PVDF shows an expected cycle stability with almost no capacity decay after 200 cycles at 5C, it delivers significantly lower capacity than that of LFP–PI at the same rate (Figure 4c). It should be noted that the capacity of LFP–PI gradually increases in the first few cycles because of the active process of PI binders, and the specific capacity after stabilization is 40% higher than that of LFP–PVDF. Besides, the LFP–PI also exhibits superior cycling stability with the capacity retention as high as 98% after 200 cycles compared to the stabilized capacity after active process. To further explore the influence of different binders on the reaction kinetics of LFP electrodes, the Li-ion diffusion coefficients (D_{Li}^{+}) of LFP–PVDF and LFP–PI were measured through EIS [46]. Figure 4d shows the fitting curves of Z_{Im} and $\omega^{-0.5}$ for LFP–PVDF and LFP–PI electrodes. The D_{Li}^{+} of the two electrodes can be calculated according to the following formula: $D_{Li}^{+} = R^2T^2/(2A^2n^4F^4c^2\sigma^2)$, where R is the ideal gas constant (8.314 J mol^{-1} K^{-1}), T is the absolute temperature, A is the surface area of the active material (cm^2), n is the transferred electron number during the electrochemical reaction, and F is the Faraday constant (96,485 C mol^{-1}). Benefiting from the high ion conductivity and electrochemical activity of PI binder, LFP–PI exhibits a significantly enhanced D_{Li}^{+} of 8.00×10^{-14} cm^2 s^{-1}, larger than that of LFP–PVDF (2.19×10^{-14} cm^2 s^{-1}).

To verify the stability of PI binder in organic electrolyte, the PI and PVDF powders are immersed into the 1 M $LiPF_6$ in EC/DMC/EMC electrolyte as shown in Figure 5a. PVDF quickly settled to the bottom of the electrolyte when it was immersed, suggesting a poorer dispersibility. In contrast, the PI binder exhibits uniform dispersion and forms yellow suspension without obvious sedimentation at the beginning of immersing. As the time increased to 24 h, the electrolyte gradually appeared delaminated with a slight sedimentation, and the amount of PI sedimentation did not continue to increase significantly until the immersing time was extended to 48 h. The morphology changes of PI and PVDF powders after immersion in the electrolyte for 48 h were further investigated as shown in Figure 5b and c. Spherical-like PVDF particles with smooth surface cracked into irregular agglomerate after swelling in the organic electrolyte [42]. However, the PI almost maintains the original morphology with similar particle size after immersing in the electrolyte compared to that of the pristine PI powder (Figure 1f). The above results indicate that the PI binder possesses superior dispersion and structural stability in organic electrolyte. SEM images of the two electrode films after cycling test were also analyzed to verify the superior stability of PI binders (Figure 5d and e). Obviously, LFP–PI

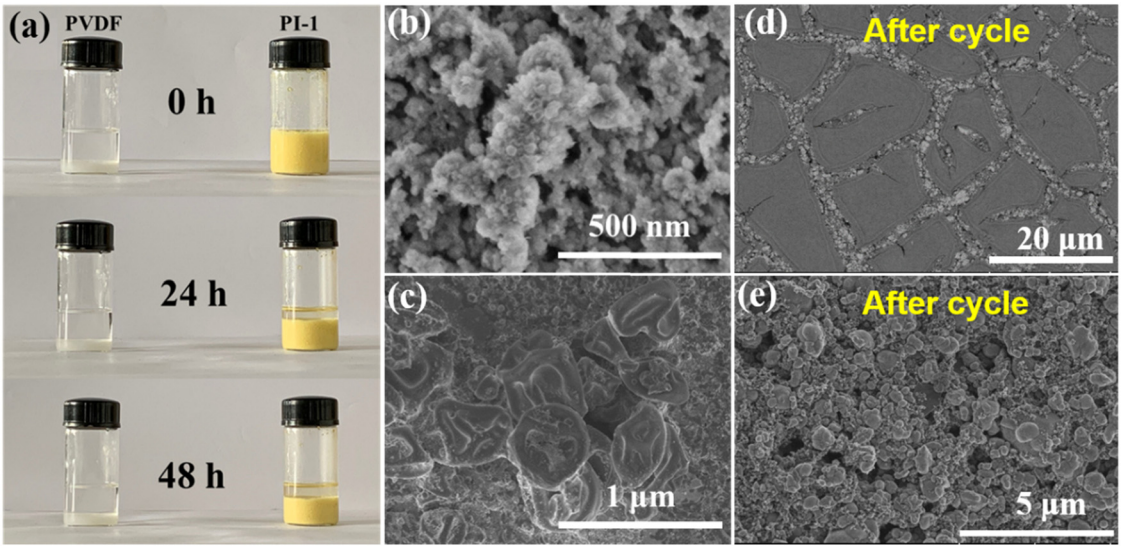

Figure 5: (a) Digital photographs of PVDF and PI powders after immersing in the electrolyte for different times; SEM images of (b) PVDF and (c) PI powders after immersing in electrolyte for 48 h; SEM images of (d) LFP–PVDF and (e) LFP–PI electrode films after cycling test.

electrode shows similar morphology with the fresh electrode (Figure 3d). LFP–PVDF electrode shows manifest re-aggregation during cycling, which can be attributed to the failure morphology of PVDF binder in the electrolyte, leading to the significant reduction of its adhesive ability.

Although the PI binder exhibits excellent stability in the organic electrolyte and contributes to additional capacity based on the reversible reaction of carbonyl groups, there is still a long way to completely replace the commercial PVDF binder. For example, the physical properties such as adhesion strength, ductility, tensile, and electrolyte uptake of PI are necessary to be deeply investigated to optimize the binder content and electrode manufacturing process. The physical/chemical changes of PI binder during the charge–discharge process should be carefully monitored through theoretical and experimental methods. Besides, the influence of molecular weight and chain structure on the adhesive performance also needs further exploration in terms of the structural diversity of PI. Therefore, the implementation of PI-PVDF hybrid binder by combining the advantages of each provides a possible alternative to develop high energy density LIBs. Figure 6 shows the electrochemical performances of three PI-PVDF hybrid binders with different PI content (30, 50, and 70 wt%) accounting for the total binder content (10 wt%) in the electrode components. When the rate increased from 0.2C to 5C, the LFP–PI electrodes show gradually promoted capacity retention of 27.1% (LFP–PI-0.3), 30.8% (LFP–PI-0.5), and 50.4% (LFP–PI-0.7) with the increase in PI content (Figure 6a). The reversible capacities of LFP–PI-0.5 and LFP–PI-0.7 are much higher than that of LFP–PI-0.3 at a small rate of 0.2C, further verifying that the incorporation of PI with high ion conductivity and electrochemical activity in PVDF binder during the electrode fabrication process can elevate the energy density of LFP electrode. Moreover, all the LFP–PI-0.3, LFP–PI-0.5, and LFP–PI-0.7 electrodes exhibit superior cycling stability during 300 cycles at 1C after the first few cycles of activation with the stabilized reversible capacities of 128, 134, and 141 mA h g^{-1}, respectively (Figure 6b). The above results suggest that the PI binder can not only contribute extra capacity and accelerate the electrochemical reaction kinetics of the LFP electrode, but also maintain good bonding stability during long cycling.

4 Conclusion

A multifunctional PI was successfully synthesized through a facile hydrothermal polymerization method and served as a binder for commercial LFP cathode. Compared to the traditional PVDF binder, the PI binder serves as the effective bridges between active particles with stable distribution while boosting ion diffusion through the electrode. The high dispersion stability of PI in NMP can effectively prevent the re-aggregation of active particles during the repeated charge–discharge processes. Moreover, the active carbonyl groups existing in the PI skeleton also can contribute to an extra capacity based on the reversible enolization reaction. The multifunction of PI can synergistically improve the capacity and rate performance of the LFP electrode. Thus LFP–PI electrode shows larger capacity and better rate capability compared with LFP–PVDF electrode. Meanwhile, the PI also can maintain well dispersion stability in the organic electrolyte, endowing LFP–PI electrode with great cycling

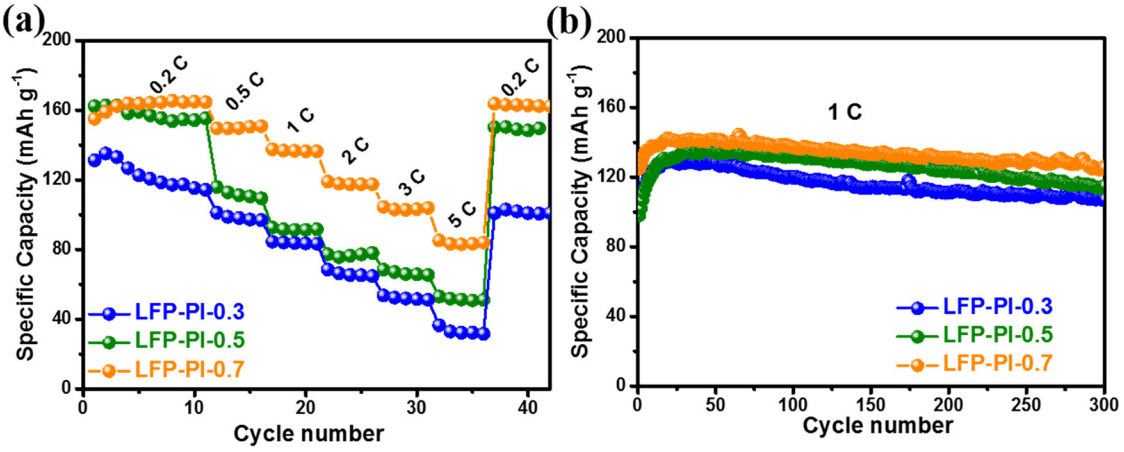

Figure 6: (a) Rate capabilities and (b) cycling performances at 1C of LFP–PI-0.3, LFP–PI-0.5, and LFP–PI-0.7 electrodes.

stability compared to the LFP–PVDF electrode. This work offers a new view for developing high-safety and high energy density LFP batteries.

Acknowledgments: This work was supported by the National Natural Science Foundation of China (51902349), Hubei Provincial Natural Science Foundation of China (2019CFB260), and Fundamental Research Funds for Central Universities (CZP19001 and CZQ19003).

Conflict of interest: The authors declare no conflicts of interest regarding the publication of this paper.

References

[1] Lin DC, Liu YY, Cui Y. Reviving the lithium metal anode for high-energy batteries. Nat Nanotechnol. 2017;12(3):194–206.
[2] Liao CY, Zhang Q, Zhai TY, Li HQ, Zhou HS. Development and perspective of the insertion anode Li_3VO_4 for lithium-ion batteries. Energy Storage Mater. 2017;7:17–31.
[3] Han XY, Li R, Qiu SQ, Zhang XF, Zhang Q, Yang YK. Sonochemistry-enabled uniform coupling of SnO_2 nanocrystals with graphene sheets as anode materials for lithium-ion batteries. RSC Adv. 2019;9(11):5942–7.
[4] Pan YS, Xu K, Wu CL. Recent progress in supercapacitors based on the advanced carbon electrodes. Nanotechnol Rev. 2019;8(1):299–314.
[5] Jiang YL, He CE, Qiu SQ, Zhang JL, Wang XG, Yang YK. Scalable mechanochemical coupling of homogeneous Co_3O_4 nanocrystals onto *in situ* exfoliated graphene sheets for asymmetric supercapacitors. Chem Eng J. 2020;397:125503.
[6] Kumari N, Patel SR, Gohel JV. Current progress and future prospective of perovskite solar cells: a comprehensive review. Rev Adv Mater Sci. 2018;53(2):161–86.
[7] Orlova TS, Shpeizman VV, Glebova NV, Nechitailov AA, Spitsyn AA, Ponomarev DA, et al. Environmentally friendly monolithic highly-porous biocarbons as binder-free supercapacitor electrodes. Rev Adv Mater Sci. 2018;55(1):50–60.
[8] Li ZH, Xu K, Pan YS. Recent development of supercapacitor electrode based on carbon materials. Nanotechnol Rev. 2019;8(1):35–49.
[9] Wang JJ, Sun XL. Olivine $LiFePO_4$: the remaining challenges for future energy storage. Energy Environ Sci. 2015;8(4):1110–38.
[10] Wang JJ, Sun XL. Understanding and recent development of carbon coating on $LiFePO_4$ cathode materials for lithium-ion batteries. Energy Environ Sci. 2012;5(1):5163–85.
[11] Yu F, Zhang LL, Li YC, An YX, Zhu MY, Dai B. Mechanism studies of $LiFePO_4$ cathode material: lithiation/delithiation process, electrochemical modification and synthetic reaction. RSC Adv. 2014;4(97):54576–602.
[12] Ohmer N, Fenk B, Samuelis D, Chen CC, Maier J, Weigand M, et al. Phase evolution in single-crystalline $LiFePO_4$ followed by in situ scanning X-ray microscopy of a micrometre-sized battery. Nat Commun. 2015;6:6045–51.
[13] Wang JJ, Yang JL, Tang YJ, Liu J, Zhang Y, Liang GX, et al. Size-dependent surface phase change of lithium iron phosphate during carbon coating. Nat Commun. 2014;5:3415–22.
[14] Liang YC, Wen KC, Mao YW, Liu ZP, Zhu GL, Yang F, et al. Shape and size control of $LiFePO_4$ for high-performance lithium-ion batteries. ChemElectroChem. 2015;2(9):1227–37.
[15] Ha SH, Lee YJ. Core-shell $LiFePO_4$/carbon-coated reduced graphene oxide hybrids for high-power lithium-ion battery cathodes. Chemistry. 2015;21(5):2132–8.
[16] Kapaev RR, Novikova SA, Chekannikov AA, Gryzlov DY, Kulova TL, Skundin AM, et al. Effect of carbon sources and synthesis conditions on the $LiFePO_4$/C cathode properties. Rev Adv Mater Sci. 2018;57(2):183–92.
[17] Ghouri ZK, Motlak M, Afaq S, Barakat NA, Abdala A. Template-free synthesis of Se-nanorods-rGO nanocomposite for application in supercapacitors. Nanotechnol Rev. 2019;8(1):661–70.
[18] Zou F, Manthiram A. A review of the design of advanced binders for high-performance batteries. Adv Energy Mater. 2020;10(45):2002508.
[19] Mantia FL, Huggins RA, Cui Y. Oxidation processes on conducting carbon additives for lithium-ion batteries. J Appl Electrochem. 2013;43(1):1–7.
[20] Ye YS, Chou LY, Liu YY, Wang HS, Lee HK, Huang WX, et al. Ultralight and fire-extinguishing current collectors for high-energy and high-safety lithium-ion batteries. Nat Energy. 2020;5(10):786–93.
[21] Ventrapragada LK, Creager SE, Rao AM, Podila R. Carbon nanotubes coated paper as current collectors for secondary li-ion batteries. Nanotechnol Rev. 2019;8(1):18–23.
[22] Pasha BA, Kaleemulla M. Processing and characterization of aluminum metal matrix composites: an overview. Rev Adv Mater Sci. 2018;56(1):79–90.
[23] Chen H, Ling M, Hencz L, Ling HY, Li GR, Lin Z, et al. Exploring chemical, mechanical, and electrical functionalities of binders for advanced energy-storage devices. Chem Rev. 2018;118(18):8936–82.
[24] Hwang SS, Sohn M, Park HI, Choi JM, Cho CG, Kim H. Effect of the heat treatment on the dimensional stability of Si electrodes with PVDF binder. Electrochim Acta. 2016;211:356–63.
[25] Xu JT, Chou SL, Gu QF, Liu HK, Dou SX. The effect of different binders on electrochemical properties of $LiNi_{1/3}Mn_{1/3}Co_{1/3}O_2$ cathode material in lithium ion batteries. J Power Sources. 2013;225:172–8.
[26] Liu YF, Jiang LY, Wang HN, Wang H, Jiao W, Chen GZ, et al. A brief review for fluorinated carbon: synthesis, properties and applications. Nanotechnol Rev. 2019;8(1):573–86.
[27] Kim JS, Choi WC, Cho KY, Byun DJ, Lim JC, Lee JK. Effect of polyimide binder on electrochemical characteristics of surface-modified silicon anode for lithium ion batteries. J Power Sources. 2013;244:521–6.
[28] Thompson L, Azadmanjiri J, Nikzad M, Sbarski I, Wang J, Yu AM. Cellulose nanocrystals: production, functionalization and advanced applications. Rev Adv Mater Sci. 2019;58(1):1–16.
[29] Lee JH, Paik U, Hackley VA, Choi YM. Effect of poly(acrylic acid) on adhesion strength and electrochemical performance of natural graphite negative electrode for lithium-ion batteries. J Power Sources. 2006;161(1):612–6.

[30] Li J, Le DB, Ferguson PP, Dahn JR. Lithium polyacrylate as a binder for tin–cobalt–carbon negative electrodes in lithium-ion batteries. Electrochim Acta. 2010;55(8):2991–5.
[31] Liu TF, Tong CJ, Wang B, Liu LM, Zhang SQ, Lin Z, et al. Trifunctional electrode additive for high active material content and volumetric lithium-ion electrode densities. Adv Energy Mater. 2019;9(10):1803390.
[32] Uchida S, Mihashi M, Yamagata M, Ishikawa M. Electrochemical properties of non-nano-silicon negative electrodes prepared with a polyimide binder. J Power Sources. 2015;273:118–22.
[33] Choi J, Kim K, Jeong J, Cho KY, Ryou MH, Lee YM. Highly adhesive and soluble copolyimide binder: Improving the long-term cycle life of silicon anodes in lithium-ion batteries. ACS Appl Mater Interfaces. 2015;7(27):14851–8.
[34] Yao DH, Yang Y, Deng YH, Wang CY. Flexible polyimides through one-pot synthesis as water-soluble binders for silicon anodes in lithium ion batteries. J Power Sources. 2018;379:26–32.
[35] Pham HQ, Kim G, Jung HM, Song SW. Fluorinated polyimide as a novel high-voltage binder for high-capacity cathode of lithium-ion batteries. Adv Funct Mater. 2018; 28(2):1704690.
[36] Zhang XF, Cui X, Lu CH, Li H, Zhang Q, He CE, et al. Conjugated polyimide-coated carbon nanofiber aerogels in a redox electrolyte for binder-free supercapacitors. Chem Eng J. 2020;401:126031.
[37] Zhang Q, Lin GY, He Y, Cui X, Yang YK. Chain engineering-tailored microstructures and lithium storage performance of hydrothermally-synthesized linear polyimides. Mater Today Chem. 2020;17:100341.
[38] Baumgartner B, Bojdys MJ, Unterlass MM. Geomimetics for green polymer synthesis: highly ordered polyimides via hydrothermal techniques. Polym Chem. 2014;5(12):3771–6.
[39] He Y, Li H, Zhang Q, He CE, Zhang XF, Yang YK. Homogeneous coating of carbon nanotubes with tailored N-doped carbon layers for improved electrochemical energy storage. RSC Adv. 2019;9(70):40933–9.
[40] Liu X, Qiu SQ, Mei P, Zhang Q, Yang YK. Chain structure-dependent electrochemical performance of polyimide cathode materials for lithium-ion batteries. J Mater Sci. 2021;56:3900–10.
[41] Song ZP, Zhan H, Zhou YH. Polyimides: promising energy-storage materials. Angew Chem Int Ed. 2010;49(45):8444–8.
[42] Qian GN, Wang L, Shang YM, He XM, Tang SF, Liu M, et al. Polyimide binder: a facile way to improve safety of lithium ion batteries. Electrochim Acta. 2016;187:113–8.
[43] Wang JJ, Chen-Wiegart YK, Wang J. In operando tracking phase transformation evolution of lithium iron phosphate with hard X-ray microscopy. Nat Commun. 2014;5:4570–9.
[44] Cho JH, Park JH, Lee MH, Song HK, Lee SY. A polymer electrolyte-skinned active material strategy toward high-voltage lithium ion batteries: a polyimide-coated $LiNi_{0.5}Mn_{1.5}O_4$ spinel cathode material case. Energy Environ Sci. 2012;5(5):7124–31.
[45] Wang H, Yao CJ, Nie HJ, Wang KZ, Zhong YW, Chen PW, et al. Recent progress in carbonyl-based organic polymers as promising electrode materials for lithium-ion batteries (LIBs). J Mater Chem A. 2020;8(24):11906–22.
[46] Zhang Q, He Y, Mei P, Cui X, Yang YK, Lin ZQ. Multi-functional PEDOT-engineered sodium titanate nanowires for sodium-ion batteries with synchronous improvements in rate capability and structural stability. J Mater Chem A. 2019;7:19241–7.